

Contents list available at CBIORE journal website

Renewable Energy Development

Journal homepage: https://ijred.cbiore.id



Research Article

A numerical H Darrieus hydrokinetic turbine performance assessment with the application of openings in blade geometry

Mateo Arrieta Gomez^{*}, Angie Guevara-Muñoz, Diego Hincapie Zuluaga

Department of Engineering, Instituto Tecnológico Metropolitano, Medellín, Colombia

Abstract. This study explores the impact of various geometric modifications, including leading-edge openings, trailing- edge openings, and circular openings, on the performance of the H Darrieus hydrokinetic turbine. These modifications involved the removal of material from a symmetrical NACA0018 airfoil along its surface. The leading edge and trailing edge openings extended from the lower to the upper surface of the blade, while the circular opening was applied exclusively to the upper surface. Using the commercial software ANSYS® V22.2, the turbine was designed, discretized, and analyzed through computational fluid dynamics employing the Realizable K-e turbulence model. The primary output variable measured was torque, from which the power coefficient for each design modification was derived, allowing for the calculation of efficiency in each scenario. Notably, the configuration featuring the upper circular opening achieved the highest efficiency at 51.88% at a Tip Speed Ratio (TSR) of 2.0, a significant improvement over the standard case which had an efficiency of 45.16%. In contrast, the leading-edge and trailing-edge openings resulted in reduced efficiencies of 44.54% and 31.19%, respectively. The enhanced power coefficient of the H Darrieus hydrokinetic turbine with circular openings is attributed to the increased pressure difference generated between the upper and lower surfaces of the blade, surpassing the performance of the standard design.

Keywords: CFD, H Darrieus, Geometrical modifications, Efficiency.



@ The author(s). Published by CBIORE. This is an open access article under the CC BY-SA license (http://creativecommons.org/licenses/by-sa/4.0/).

Received: 20th July 2024; Revised: 18th Oct 2024; Accepted: 7th Nov 2024; Available online: 25th Nov 2024

1. Introduction

As the global population continues to expand, so does the demand for energy. This increasing need is primarily satisfied through the combustion of fossil fuels, resulting in heightened pollution levels and the accelerated depletion of these finite resources (Hussain et al., 2019; Khan et al., 2021; La Camera, n.d.; Welsby et al., 2021). Currently, fossil fuels account for 60% of electricity generation worldwide, while renewable sources such as solar and wind contribute 34%, and nuclear power represents 6% (Renewable Energy Agency, 2023).

Colombia has witnessed a notable surge in electrical energy demand, with an impressive increase of 3.72% in February 2022 compared to the same month in 2021 (XM, 2022). However, a staggering 53% of the nation's territory, primarily rural and remote areas, remains disconnected from the national energy grid (IPSE, 2022). Studies reveal that connecting these remote regions to the grid poses significant transportation challenges (Dyner et al., 2005). One promising solution to alleviate the energy shortfall in these areas is the installation of small hydroelectric power plants, commonly referred to as small hydro. A small hydro is an energy generating hydroelectric plant between 1MW and 10MW. These plants could operate in the nearest water stream to the remote area (Julian et al., 2017). Nevertheless, due to difficulties in access to these areas, high cost of installation and maintenance, and the negative environmental impacts the construction of a small hydro plant is discarded (Briones Hidrovo et al., 2017; Yadav et al., 2023). The challenges of bringing power to the remote areas have led to an increased research and development of non-conventional hydrokinetic turbines (Chaulagain et al., 2023; Tan et al., 2021; Yadav et al., 2023). Several studies are focused on the development of low-cost efficient turbines that are easy to install and maintain (Vargas et al., 2016). In this case, the H Darrieus hydrokinetic turbine is ideal for manufacturing, transporting, and installing in small or difficult-to-reach rivers (Bilgili et al., 2018; Kirke, 2020). The application of an H Darrieus turbine represents a promising solution to fulfill the demand for electricity supply (at least for one household) in remote areas due to its affordability and straightforwardness of installation.

1.1. H Darrieus Hydrokinetic Turbine

The H Darrieus turbine is an electrical energy generator that is commonly used in converting air kinetic energy to mechanical energy, but thanks to its fluid dynamics principles it can be used in water streams. This turbine, as seen in Fig 2, is made up of two or more blades (three in this case) that generate a rotation when a pressure difference is created when the water flows over the same blades (Rehman et al., 2018). The rotation in the vertical axis removes the need of submerging mechanical systems or transition systems into the water.

Email: mateoarrieta263398@correo.itm.edu.com (M.A.Gomez)

Corresponding autor:

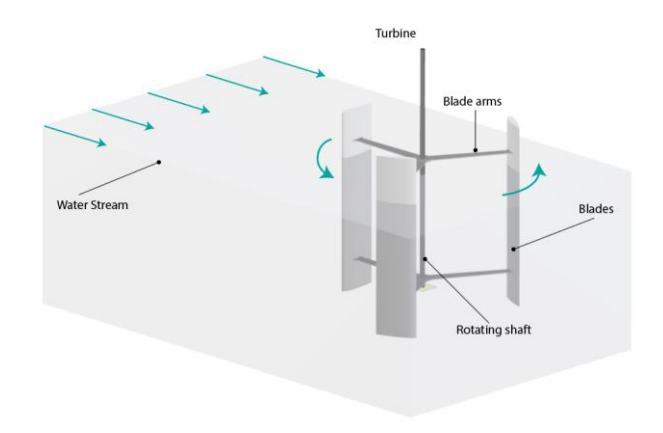


Fig 2. H Darrieus turbine in a water stream

The H Darrieus turbine doesn't need oversized civil constructions like canals or a dam because of its ability of using the natural flow of the water streams, therefore, it is suitable for applications in difficult access zones. Nevertheless, this turbine presents low efficiencies in comparison with the conventional turbines in hydroelectric plants, namely, Pelton, Francis, and Kaplan (Halder *et al.*, 2021; Liu *et al.*, 2015; Quaranta & Trivedi, 2021). Because of this, studies have been carried out with the purpose of increasing the energy generation.

1.2. Performance Enhancement

Numerous approaches exist to improve the efficiency of the H Darrieus hydrokinetic turbine, including parametric configurations, passive elements, array designs, and geometric modifications. Research has demonstrated that altering the cross-sectional area of the blade profile significantly impacts the turbine's performance, confirming the influence of these modifications on the H Darrieus turbine's efficiency (Mohamed, 2012).

One effective modification method involves the addition of material. Gonçalves et al. (2022) conducted experimental studies on the inclusion of protuberances on the trailing edge of blades, successfully enhancing self-starting capability and reducing stall. Tigabu et al. (2022) explored how inertia affects the self-starting capacity of turbines, revealing an inverse relationship between self-starting acceleration and torque overshoot. Additionally, López et al. (2024) investigated the impact of a winglet positioned atop a Darrieus blade. Their study began with an analysis of the optimal cant angle for the winglet, followed by a subsequent examination of the sweep angle while maintaining fixed dimensions for the winglet's height and chord length. The optimal winglet configuration was achieved with a cant angle of 45° and a sweep angle of 60°, resulting in a remarkable 20% increase in the power coefficient compared to scenarios without winglets. Additionally, significant modifications to Savonius-type turbines were introduced, as documented by Shashikumar & Madav (2021). Their numerical simulations explored the performance of modified rotors featuring "V"-shaped blades at angles varying from 90° to 40°, revealing that an angle of 80° yielded the highest power coefficient of 0.2279 at a tip speed ratio (TSR) of 0.9. Furthermore, López et al. (2024) enhanced the blade's trailing edge by incorporating a Gurney Flap at 2% of the chord length (C) inclined at 45° inward. This innovative adjustment resulted in a 10.7% increase in the power coefficient compared to standard smooth blades.

Ibrahim *et al.* (2022) examined the effects of removing material by introducing a circular opening in the lower surface of the Darrieus blade. Their findings revealed a notable enhancement in the turbine's performance, achieving a power coefficient of 0.435 at a tip speed ratio (TSR) of 2.3. In contrast to the extensive research on material addition, the investigation into material removal remains relatively underexplored. This paper seeks to enhance the energy output of a Darrieus hydrokinetic turbine by incorporating geometric modifications via material removal. Specifically, it examines the effects of leading-edge openings, trailing edge openings, and circular openings on the blades of H Darrieus turbines through computational fluid dynamics analysis.

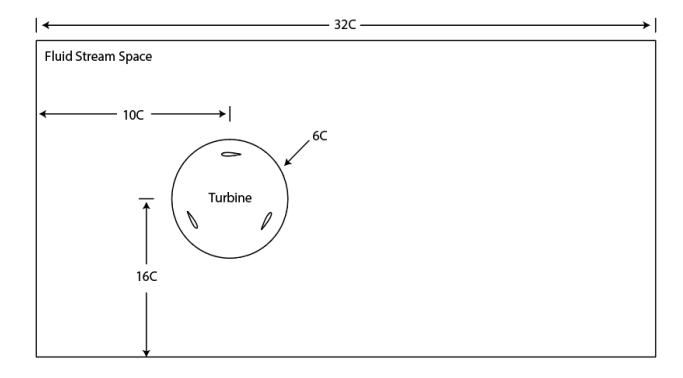
2. Methodology

2.1. H Darrieus turbine design

The general design of the system consisted of the fluid's stream space (static domain) and the turbine (rotary domain). The measurements of the system were configured as in function of the blades chord length (C). the measurements of the system were maintained constant for all the modification cases because this work only modified the design of the blades. The measurement of the domains in function with the blades chord length is shown in Fig 1.

The design module SpaceClaim was used to generate the blade's geometry. For this work five different types of modification were carried out from the standard case design. The standard case design, as shown in Fig 3.a corresponds to a NACA 0018 Profile. This is a symmetrical airfoil and it was chosen because of its wide use in fluid dynamics studies (Rogowski *et al.*, 2021).

The chord length (C) of the standard case was adjusted to 200 mm and was maintained for the rest of the modification cases. A blade with circular opening (CO) in its upper surface was designed, as seen in Fig 3.b. The position and size opening were adjusted with independent parameters that are W_1 , W_2 and L. An additional modification was the leading-edge openings (LEO) as shown in Fig 3.c. Two different designs of this type of modifications were done with different parameters, including the angle of the opening α . The last modification of this type was this same opening but near the trailing edge (TEO), as seen in Fig 3.d and two different designs were also carried out. The design parameters for all cases are shown in Table 1. The values of this parameters were arbitrarily chosen and the difference between LEO #1 and #2 are a proportional scale and a slight change in the angle of the opening. The same modification was done between the TEO #1 and TEO #2. A roundness or curvatures at the inlet and outlet of the surfaces in



 $\textbf{Fig 1.} \ Design \ parameters \ of the \ H \ Darrieus \ turbine \ system \ simulation$

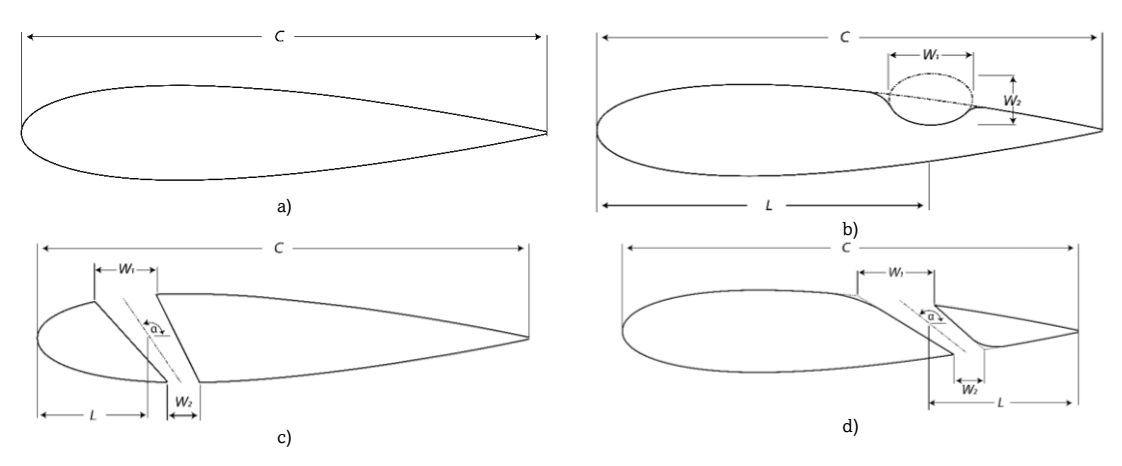


Fig 3. Design guide a) standard case b) CO c) LEO d) TEO

Table 1

Design parameters for all modification cases							
Design	W ₁ (mm)	W ₂ (mm)	L (mm)	a (°)			
Standard	-	-	-	-			
CO	42	16	120	-			
LEO #1	30	14	60	140			
LEO #2	36	18	60	150			
TEO #1	30	14	70	140			
TEO #2	36	15	70	150			

the modifications was also considered and applied with a tangent constrain.

2.2. Discretization

The meshing module called ICEM CFD of the commercial software ANSYS ® V22.2. was used to generate the finite elements of all the modification cases. The general mesh was

done in two parts: the static domain (as seen in Fig 5.a) and the rotary domain (as seen in Fig 5.b). The rotary domain was done with smaller-sized elements compared to the static domain. The two domains were discretized with structured meshes in order to allow for a faster and more accurate fluid dynamic assessment (He *et al.*, 2024). The number of elements were kept around 137106 in order to achieve results independent of mesh

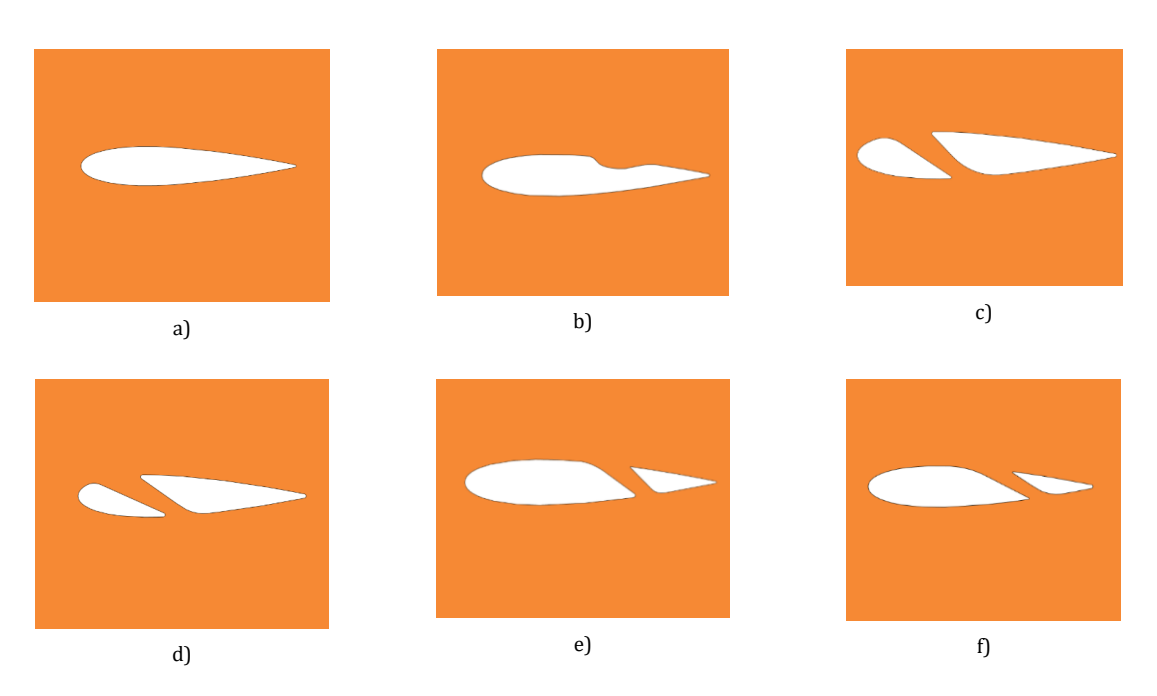


Fig 4. Designs carried out in SpaceClaim a) Standard b) CO c) LEO #1 d) LEO #2 e) TEO #1 f) TEO #2.

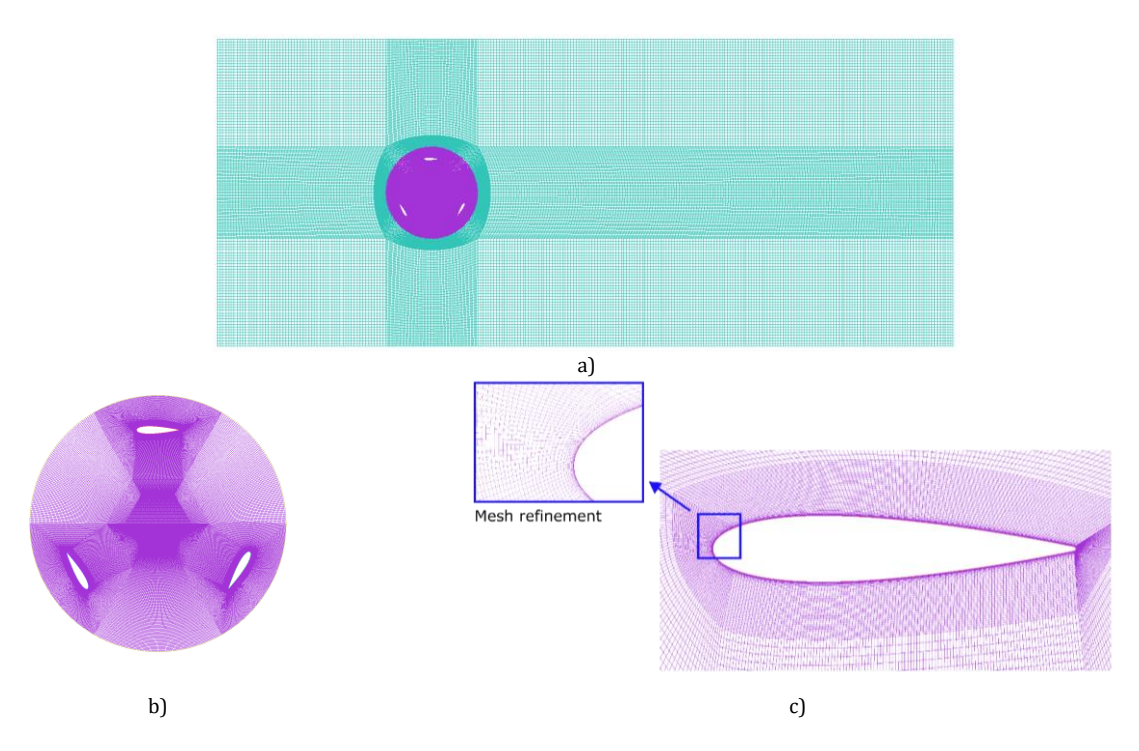


Fig 5. Detailed illustration of the a) system mesh a) rotary domain mesh b) refined mesh near the edge of the blade.

elements number, as it was similarly done in the work of Saini & Saini (2018). The mesh near the edge of the blades, as seen in Fig 5.c, was refined using a Y+, with an element growth of 1.2, with the objective of obtaining precise results in the viscous zone of the blade (Yunus Cengel, 2006). Fig 4 shows the design carried out in SpaceClaim for every study case.

2.3. Boundary conditions and numerical configuration

The study's procedure was conducted using the Fluent module of the commercial software ANSYS® V22.2. The boundary conditions had been previously defined in the finite element generation module, ICEM. The system domains consisted entirely of liquid water throughout the simulation, indicating that both the static and rotary domains were immersed in flowing water. The fluid velocity was established at 1 m/s at the canal's inlet, a standard value referenced in previous studies (Kamal & Saini, 2023; Liang et al., 2017a; Saini & Saini, 2020), with an outlet pressure set to 0 Pa. Additionally, this module incorporates sliding meshes via an interface to connect the static and rotary domains, as illustrated in Fig 6. In each study case, the angular velocity of the rotary domain varies from 2.22 to 7.77 rad/s to achieve tip speed ratios (TSR) of 1.0, 1.5, 2.0, and 2.5. The simulation duration was set to 10 seconds, yielding 2000 samples (steps) with a sampling interval of 0.005 seconds, as recommended by Guevara-Muñoz et al. (2023). This timestep size was sufficient for the system to produce reliable and accurate results.

The Realizable K- ϵ turbulence model had been selected for the simulation due to its exceptional accuracy in predicting flows characterized by rotation and swirling motion (Liang *et al.*, 2017b; Mohamed, 2012; Mohamed *et al.*, 2015). The parameters previously mentioned are detailed in Table 2.

2.4. Turbulence model equations

The fluid dynamics solver is based on the Navier Stokes equations, and these equations are simplified to the Reynolds-Averaged Navier Stokes (RANS) equations. These equations allow the turbulence effects to be added to the Navier-Stokes equations. The tensor form of this operation is shown:

$$\frac{\partial(\rho U_i)}{\partial t} + \frac{\partial(\rho U_i U_j)}{\partial x_j} = -\frac{\partial p}{\partial x_i} + \frac{\partial}{\partial x_j} \left[\mu(\frac{\partial U_i}{\partial x_j} + \frac{\partial U_j}{\partial x_i}) - \overline{\rho u_i' u_j'} \right] \tag{1}$$

Where ρ is the density, p is the static pressure, U is the mean velocity flow, u' velocity fluctuation due to turbulence and $\overline{\rho u_l' u_j'}$ Reynolds stress term. This process results in the addition of the Reynolds stress term. To solve the equation the Reynolds stress term must be expressed in mean flow velocity quantities:

$$\overline{\rho u_i' u_j'} = \mu_t \left(\frac{\partial u_i}{\partial x_j} + \frac{\partial u_j}{\partial x_i} - \frac{2}{3} \frac{\partial u_k}{\partial x_k} \delta_{ij} \right) - \frac{2}{3} \rho k \delta_{ij}$$
 (2)

where μ_t is the turbulent viscosity δ_{ij} is the Kronecker delta.

The K-epsilon RNG turbulence model is added to the RANS equations as has been done in several works focused on similar cases (El-Askary *et al.*, 2018; Lee *et al.*, 2016; Saad *et al.*, 2017). This turbulence model allows capturing the effect of vortices in the flow and is sensitive to the flow stresses experienced by the rotor at higher angular velocities (Yakhot *et al.*, 1992). The turbulence kinetic energy (k) is described in equation 3 and the dissipation rate (ϵ) is given in Eq. (3) and Eq. (4):

$$\rho \frac{Dk}{Dt} = \frac{\partial}{\partial x_i} \left(\alpha_k \mu_{cff} \frac{\partial k}{\partial x_i} \right) + G_k - \rho \varepsilon \tag{3}$$

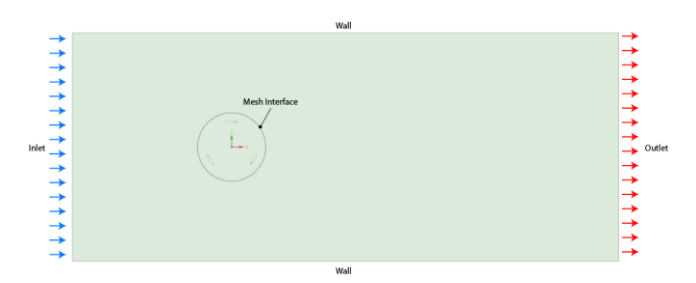


Fig 6. Boundary conditions settings

Table 2 Simulation Parameters

Parameter	Value	
Type of Simulation	imulation Transitory	
Inlet Velocity	1 [m/s]	
Angular Velocity	2.22 [rad/s] - 7.77 [rad/s]	
Temperature	25°	
Output Pressure	0 Pa	

$$\rho \frac{Dk}{Dt} = \frac{\partial}{\partial x_i} \left(\alpha_k \mu_{cff} \frac{\partial k}{\partial x_i} \right) + C_{1\varepsilon} G_k \frac{\varepsilon}{k} - C_{2\varepsilon} \rho \frac{\varepsilon^2}{k} - R_{\varepsilon}$$
 (4)

where α_k and α_{ε} are the Prandtl numbers for turbulent kinetic energy (k) and dissipation rate (ε) , respectively. The value of α_k and α_{ε} are 0.7194. $C_{1\varepsilon}$ and $C_{2\varepsilon}$ are constants with a value of 1.42 and 1.68, respectively. In addition, μ_{cff} and G_k are the dispersion coefficient and turbulent kinetic energy generation due to average velocity gradients.

2.5. Performance equations

The power of the H Darrieus turbine is calculated by the equation 1, where T is the average moment of the turbine and w is the angular velocity (Douak & Aouachria, 2015).

$$P = Tw (5)$$

The power coefficient is calculated with Eq. (6), where P is the calculated power in Eq. (5), ρ is the fluids density, V the fluids velocity, R the turbines radius and H the height of the blades (Saryazdi & Boroushaki, 2018).

$$C_P = \frac{P}{\rho V^3 RH} \tag{6}$$

The tip speed ratio (TSR) of the turbine calculates the ratio between the turbine's angular velocity and the stream velocity. This measurement is needed for calculating the power coefficient (Wardhana & Fridayana, 2020), and thus, the TSR is a function of the turbine's efficiency.

$$TSR = \frac{\omega R}{V} \tag{7}$$

Where ω is the turbines angular speed. The turbines solidity is a dimensionless parameter. This one gives us the dimension form of the turbine. The solidity (σ) is the amount of blockage that the turbine causes in its swept area and in this work, it is maintained constant for all modification cases. It is defined as follows (Alqurashi & Mohamed, 2020):

$$\sigma = \frac{NC}{2R} \tag{8}$$

Where N represents the number of blades and C the blades chord length.

2.6. Mesh independency analysis

A mesh independency study was carried out to stablish the number of elements which guarantee precise and stable result. For the mesh analysis the standard case was selected and four different grids starting from 21697 elements till 242767 elements were created. Also, the torque of the turbine was stablished as the convergence variable

3. Results and Discussion

3.1. Mesh independency analysis

Fig 7 show the torque generated in the standard case in function of the number of elements. The four different meshes were plotted and the results show a tendency to a torque of 106 Nm.

From the analysis of Fig 7 meshes with a number of cells greater than 137106 cells were created for all cases because of the fact that it presents a difference of 0.46% compared to the next number of cells tested (242767). The mesh independence applies to all the other cases because of the similarities between them in terms of number of elements and quality. Table 3 shows the mesh metrics, where the minimum 2x2 determinant is supposed to be greater than 0.3, the maximum aspect ratio is

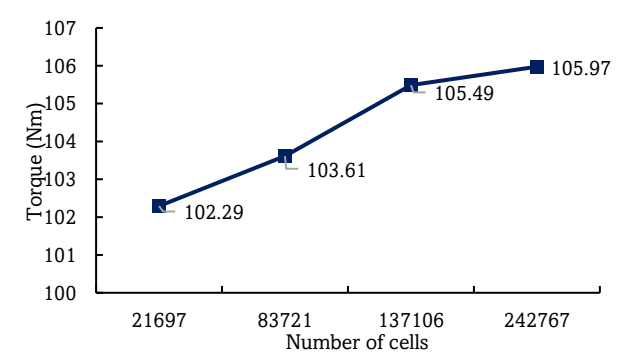


Fig 7. Mesh independency analysis results

Table 3 Mesh metrics for every case

Case	Number of cells	Min. Determinant 2x2	Max. Aspect ratio	Min. quality
Standard	183763	0.819	92.4	0.819
CO	158543	0.837	35.5	0.837
LEO #1	186237	0.668	105	0.668
LEO #2	168708	0.698	32.3	0.698
TEO #1	180842	0.791	38.4	0.791
TEO #2	197830	0.683	66.9	0.683

supposed to be lower than 100 and the minimum quality is supposed to be greater than 0.3 (Ansys Inc., 2013).

3.2. Contours and streamlines analysis

The results of pressure contours show the existing relation between the torque and the magnitude of the pressure difference caused by the interaction of the fluid with the blades. In Fig 8 we can find the pressure contours for the standard case, the CO and the TEO #1 case adjusted to a TSR of 1.5 because of being the best TSR and at an azimuth angle of 70° in which a peak of torque is generated. The pressure contour seen in the standard case shows an evenly spread high pressure in the top

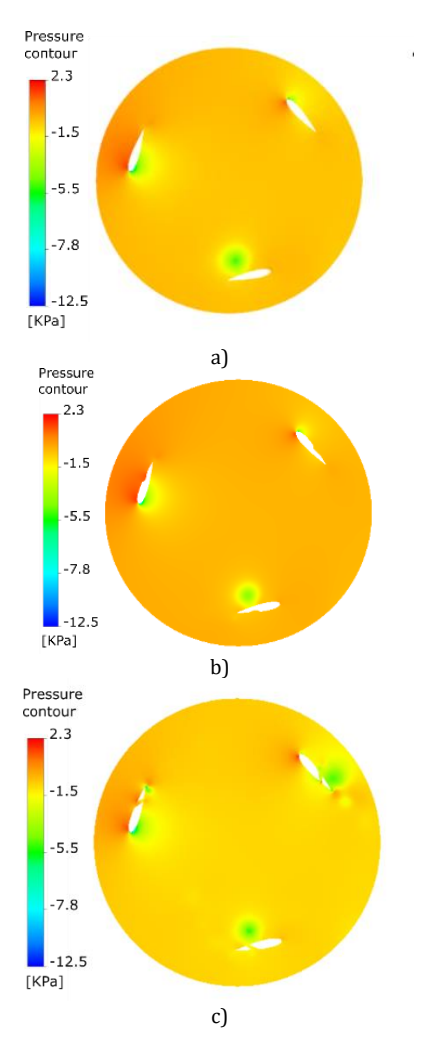


Fig 8. Pressure contours in the turbine a) standard case b) CO case c) TEO #1 case

side of the upstream blead and a lower pressure at its bottom. This translates into torque production which allows for the turbine to generate power. The same case happened for the CO case in which a continuous dispersion of high and low pressure is seen in the upper and lower surface of the blade, respectively. In the TEO #1 case it's seen that the opening causes a discontinuous dispersion of the pressure, that is, loss in lift and lower production of torque.

The analysis of pressure contours reveals the correlation between torque and the pressure difference arising from the fluid's interaction with the blades. Fig 8 illustrates the pressure contours for the standard case, as well as the CO and TEO #1 cases, both optimized for a TSR of 1.5 (the most efficient TSR) at an azimuth angle of 70°, where torque reaches its maximum. In the standard case, the pressure contour displays a consistent high-pressure zone on the upper side of the upstream blade, contrasted by lower pressure below. This pressure differential is essential for torque generation, enabling the turbine to produce power. A similar pattern was observed in the CO case, where a steady distribution of high and low pressures is evident across the blade's upper and lower surfaces. However, in the TEO #1 scenario, the presence of the opening disrupts the pressure distribution, leading to a loss in lift and a reduction in torque production. The pressure contour results reveal that the CO case exhibited the highest-pressure difference, reaching an impressive magnitude of 16388.2 Pa, as reported in the ANSYS post-processing module. This significant value indicates that the CO case is likely to generate greater torque compared to the other modification cases. To ensure the system operates correctly and to validate the interaction between the domains, we analysed a standard case that illustrates the results of the streamlines, as depicted in Fig 9. In this scenario, there is a smooth flow continuity between the two domains, with the blades serving as the sole obstacle. Additionally, the wake region exhibited a behaviour similar to Karman vortices, reinforcing the reliability of our simulations.

For the turbine to effectively harness the kinetic energy of the fluid, a more stable flow is essential to maximize energy capture by the blades. So, Fig 10 illustrates the velocity contours of both the standard case and TEO #1, highlighting the vortices produced in each scenario. The analysis was conducted

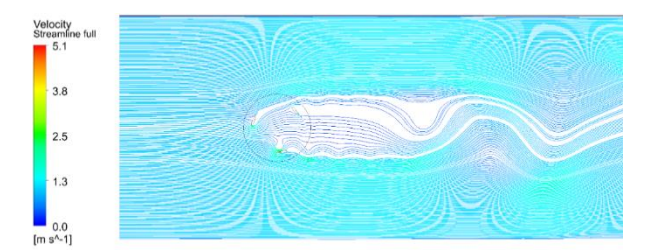


Fig 9. Streamlines of the system

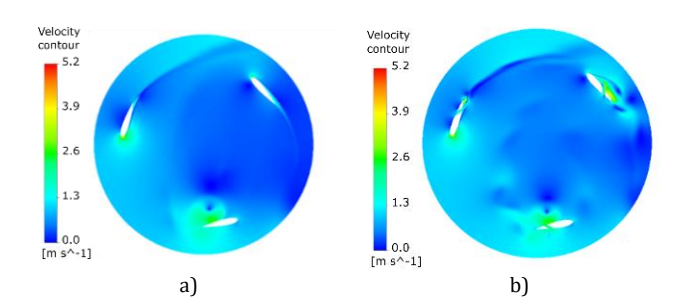


Fig 10. Velocity contours a) Standard case b) TEO #1 case

exclusively at a Tip Speed Ratio (TSR) of 1.5, as this was the TSR that showcased optimal performance. In the standard case, the flow exhibits a steadier separation and a reduced number of vortices. In contrast, TEO #1 demonstrates a more turbulent flow characterized by an increased number of vortices.

Fig 12 presents the torque coefficient graphs for both the standard and CO cases at every azimuth angle, as these represent the most favourable scenarios. These graphs illustrate the results from the turbine's final revolution. A positive torque indicates that the turbine will rotate in the desired direction (anticlockwise), while a negative torque signifies a clockwise rotation. It is noteworthy that an overall positive torque coefficient was observed for cases calibrated to a TSR of 1.5. At a TSR of 1.0, the analysis revealed inconsistent torque production at azimuth angles of approximately 120°, 240°, and 340°. This instability is attributed to the chaotic flow patterns generated at this tip speed ratio, resulting from significant flow separation occurring at lower speeds within the turbine.

3.3. Efficiency

Efficiency was calculated for each study case using the average torque and Equation (2) to assess and compare their performance. Fig 11 illustrates the efficiency achieved across all cases as a function of the Tip Speed Ratio (TSR). The CO case demonstrated a remarkably similar and higher efficiency compared to the standard case, while the other cases exhibited lower efficiency relative to the standard at TSRS of 1.5, 2.0, and

2.5. Generally, all cases achieved peak efficiency at a TSR of 2.0, except for the LEO cases, which attained their highest efficiency at a TSR of 1.5.

The most favorable outcomes were observed in the circular opening (CO) case, which demonstrated an enhancement in efficiency of 51.88% in comparison to the standard case, which recorded an efficiency of 45.16%. This improvement in efficiency may be ascribed to the circular opening's effect on increasing the blades' rotational speed, resulting in a greater pressure differential between the upper and lower surfaces of the blade, thereby generating higher torque. This observed increase in efficiency is corroborated by the findings of Ibrahim et al. (2022), in which a similar circular opening on the lower surface of the blade facilitated a greater generation of torque relative to the standard case. Conversely, in the remaining cases, notably the leading edge opening (LEO) and trailing edge opening (TEO) scenarios, a decline in efficiency was noted, with values falling below 44.54% when compared to the standard case. This decrease in efficiency is attributed to a reduced pressure differential surrounding the blades, which subsequently diminishes torque production.

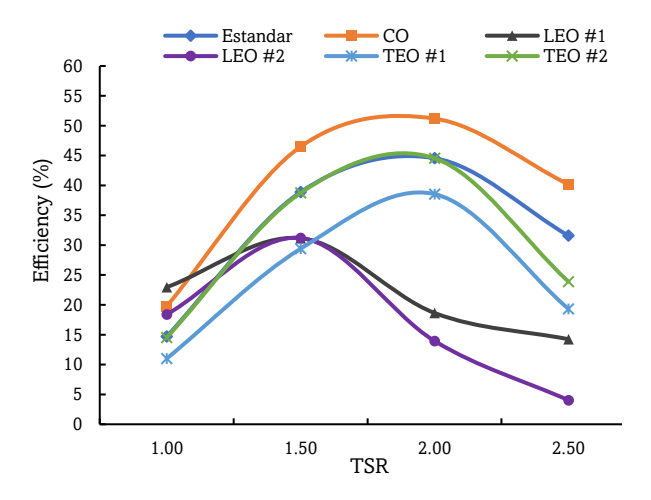


Fig 11. Efficiency results for every case in function of the TSR

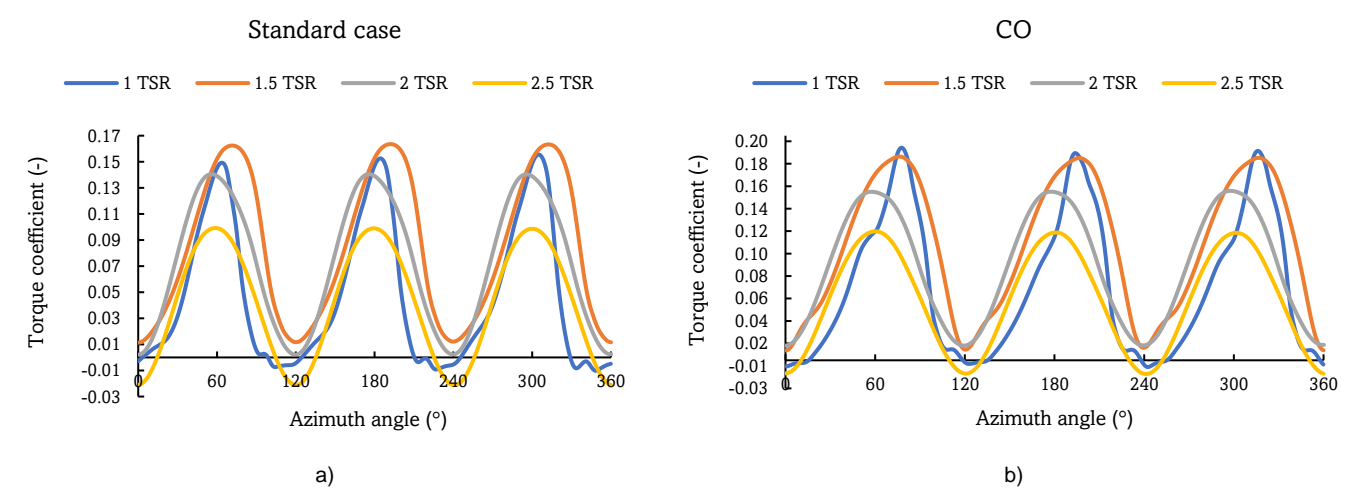


Fig 12. Torque coefficients a) standard case b) CO case

4. Conclusion

This study focused on designing and simulating the H Darrieus turbine system, incorporating various blade modifications through material removal techniques, including leading-edge openings, trailing-edge openings, and circular openings. The baseline results indicated an efficiency of 45.16%, representing the conversion of fluid kinetic energy into mechanical energy. Notably, the highest efficiency achieved among all modifications was 51.88%, observed in the circular openings case. Conversely, the trailing-edge openings modification resulted in a lower efficiency compared to the standard case, registering below 44.54%. Similarly, the leading-edge openings case demonstrated a significant decline in efficiency, falling to less than 31.19% compared to the standard. Although the TEO and LEO cases demonstrated a decrease in the efficiency of the H Darrieus turbine, their relevance in other fluid dynamics applications should not be overlooked, as these modifications can offer beneficial aerodynamic features. For future works it is proposed to use the best resulting case and to improve its efficiency by the application of external accessories (passive elements) that improve the characteristics of the liquid's flow around the turbine.

Acknowledgments

The authors express gratitude to ITM and to the Department of Computer Systems for its support with hardware, software (ANSYS V22.2 Engineering Software Licensing), and connectivity which was a central factor in the proposed project.

Author Contributions: Conceived and designed the analysis: A. Guevara. Collected the data: M. Arrieta. Contributed data or analysis tools: A. Guevara D. Hincapie. Performed the analysis: A. Guevara M. Arrieta. Wrote the paper: A. Guevara M. Arrieta.

Funding: This work was supported by the Instituto Tecnológico Metropolitano.

Conflicts of Interest: We declare that we have no significant competing interests including financial or non-financial, professional, or personal interests interfering with the full and objective presentation of the work described in this manuscript.

References

- Alqurashi, F., & Mohamed, M. H. (2020). Aerodynamic Forces Affecting the H-Rotor Darrieus Wind Turbine. *Modelling and Simulation in Engineering*, 2020, 1–15. https://doi.org/10.1155/2020/1368369
- Ansys Inc. (2013). ANSYS ICEM CFD User's Manual. 15317(November), 724–746.
- Bilgili, M., Bilirgen, H., Ozbek, A., Ekinci, F., & Demirdelen, T. (2018). The role of hydropower installations for sustainable energy development in Turkey and the world. *Renewable Energy*, 126, 755–764. https://doi.org/10.1016/J.RENENE.2018.03.089
- Briones Hidrovo, A., Uche, J., & Martínez-Gracia, A. (2017). Accounting for GHG net reservoir emissions of hydropower in Ecuador. Renewable Energy, 112, 209–221. https://doi.org/10.1016/J.RENENE.2017.05.047
- Shashikkumar, C M., & Madav, V. (2021). Numerical and experimental investigation of modified V-shaped turbine blades for hydrokinetic energy generation. *Renewable Energy*, 177, 1170–1197. https://doi.org/10.1016/J.RENENE.2021.05.086
- Chaulagain, R. K., Poudel, L., & Maharjan, S. (2023). A review on nonconventional hydropower turbines and their selection for ultra-

- low-head applications. *Heliyon*, 9(7). https://doi.org/10.1016/J.HELIYON.2023.E17753
- Douak, M., & Aouachria, Z. (2015). Starting Torque Study of Darrieus Wind Turbine. *International Journal of Mathematical, Computational, Physical, Electrical, and Computer Engineering, 9*(8), 472–477. https://doi.org/10.5281/zenodo.1108332
- Dyner, I., Alvarez, C., & Cherni, J. (2005). Energy Contribution to Sustainable Rural Livelihoods in Developing Countries: A System Dynamics Approach. https://proceedings.systemdynamics.org/2005/proceed/pape rs/DYNER155.pdf
- El-Askary, W. A., Saad, A. S., AbdelSalam, A. M., & Sakr, I. M. (2018). Investigating the performance of a twisted modified Savonius rotor. *Journal of Wind Engineering and Industrial Aerodynamics*, 182, 344–355. https://doi.org/10.1016/J.JWEIA.2018.10.009
- Gonçalves, A. N. C., Pereira, J. M. C., & Sousa, J. M. M. (2022). Passive control of dynamic stall in a H-Darrieus Vertical Axis Wind Turbine using blade leading-edge protuberances. *Applied Energy*, 324, 119700. https://doi.org/10.1016/J.APENERGY.2022.119700
- Halder, P., Doppalapudi, A. T., Azad, A. K., & Khan, M. M. K. (2021). Efficient hydroenergy conversion technologies, challenges, and policy implication. *Advances in Clean Energy Technologies*, 295–318. https://doi.org/10.1016/B978-0-12-821221-9.00007-4
- He, J. H., Li, M. G., & Chen, J. J. (2024). A novel unresolved/semiresolved CFD-DEM coupling method with dynamic unstructured mesh. *International Journal for Numerical and Analytical Methods* in Geomechanics, 48(7), 1774–1796. https://doi.org/10.1002/NAG.3701
- Hussain, A., Sarangi, G. K., Pandit, A., Ishaq, S., Mamnun, N., Ahmad, B., & Jamil, M. K. (2019). Hydropower development in the Hindu Kush Himalayan region: Issues, policies and opportunities. *Renewable and Sustainable Energy Reviews*, 107, 446–461. https://doi.org/10.1016/J.RSER.2019.03.010
- Ibrahim, A. A., Elbaz, A. M. R., Melani, P. F., Mohamed, O. S., & Bianchini, A. (2022). Power augmentation of Darrieus wind turbine blades using trapped vortex cavity. *Journal of Wind Engineering and Industrial Aerodynamics*, 223, 104949. https://doi.org/10.1016/J.JWEIA.2022.104949
- IPSE. (2022). Caracterización ZNI.
 https://ipse.gov.co/cnm/caracterizacion-energetica-de-las-zni-
- Judith Guevara-Muñoz, A., Hincapie-Zuluaga, D. A., Rodríguez-Cabal,
 M. Á., Sierra-Del-rio, J. A., Colmenares-Quintero, R. F., & Torres-Lopez,
 E. (2023). 2D Numerical Analysis of an H-Darrieus
 Hydrokinetic Turbine with Passive Improvement Mechanisms.
 Engineering Transactions, 71(4), 553–569.
 https://doi.org/10.24423/ENGTRANS.3111.20231107
- Julian, C., Acevedo, M., David, F., & Martinez, S. (2017). Diseno de una pequena central hidroelectrica para el municipo de pisba, boyaca universidad pedagogica Y tecnologica de Colombia facultad seccional duitama ingenieria electromecanica duitama, 2017. http://repositorio.uptc.edu.co/handle/001/2632
- Kamal, M. M., & Saini, R. P. (2023). Performance investigations of hybrid hydrokinetic turbine rotor with different system and operating parameters. *Energy*, 267, 126541. https://doi.org/10.1016/J.ENERGY.2022.126541
- Khan, I., Hou, F., Irfan, M., Zakari, A., & Le, H. P. (2021). Does energy trilemma a driver of economic growth? The roles of energy use, population growth, and financial development. *Renewable and Sustainable Energy Reviews*, 146, 111157. https://doi.org/10.1016/J.RSER.2021.111157
- Kirke, B. (2020). Hydrokinetic turbines for moderate sized rivers. Energy for Sustainable Development, 58, 182–195. https://doi.org/10.1016/J.ESD.2020.08.003
- La Camera, F. (n.d.). Raising climate ambitions through renewables People, Planet and Prosperity. https://www.irena.org/-/media/Files/IRENA/Agency/Publication/2019/Jul/IRENA_ People-Planet-and-Prosperity_2019.pdf
- Lee, J. H., Lee, Y. T., & Lim, H. C. (2016). Effect of twist angle on the performance of Savonius wind turbine. *Renewable Energy*, 89, 231–244. https://doi.org/10.1016/J.RENENE.2015.12.012
- Liang, X., Fu, S., Ou, B., Wu, C., Chao, C. Y. H., & Pi, K. (2017a). A computational study of the effects of the radius ratio and

- attachment angle on the performance of a Darrieus-Savonius combined wind turbine. *Renewable Energy*, *113*, 329–334. https://doi.org/10.1016/J.RENENE.2017.04.071
- Liang, X., Fu, S., Ou, B., Wu, C., Chao, C. Y. H., & Pi, K. (2017b). A computational study of the effects of the radius ratio and attachment angle on the performance of a Darrieus-Savonius combined wind turbine. *Renewable Energy*, 113, 329–334. https://doi.org/10.1016/j.renene.2017.04.071
- Liu, X., Luo, Y., Karney, B. W., & Wang, W. (2015). A selected literature review of efficiency improvements in hydraulic turbines. *Renewable and Sustainable Energy Reviews*, 51, 18–28. https://doi.org/10.1016/J.RSER.2015.06.023
- López, O. D., Botero, N., Nunez, E. E., & Laín, S. (2024). Performance Improvement of a Straight-Bladed Darrieus Hydrokinetic Turbine through Enhanced Winglet Designs. *Journal of Marine Science and Engineering 2024, Vol. 12, Page 977, 12*(6), 977. https://doi.org/10.3390/JMSE12060977
- Mohamed, M. H. (2012). Performance investigation of H-rotor Darrieus turbine with new airfoil shapes. *Energy*, 47(1), 522–530. https://doi.org/10.1016/J.ENERGY.2012.08.044
- Mohamed, M. H., Ali, A. M., & Hafiz, A. A. (2015). CFD analysis for H-rotor Darrieus turbine as a low speed wind energy converter. Engineering Science and Technology, an International Journal, 18(1), 1–13. https://doi.org/10.1016/j.jestch.2014.08.002
- Quaranta, E., & Trivedi, C. (2021). The state-of-art of design and research for Pelton turbine casing, weight estimation, counterpressure operation and scientific challenges. *Heliyon*, 7(12), e08527. https://doi.org/10.1016/J.HELIYON.2021.E08527
- Rehman, W., Rehman, F., & Malik, M. Z. (2018). A review of darrieus water turbines. *American Society of Mechanical Engineers, Power Division (Publication) POWER*, 2(March). https://doi.org/10.1115/POWER2018-7547
- Renewable Energy Agency, I. (2023). World Energy Transitions Outlook 2023: 1.5°C Pathway. www.irena.org
- Rogowski, K., Kr, G., & Bangga, G. (2021). Numerical Study on the Aerodynamic Characteristics of the NACA 0018 Airfoil at Low Reynolds Number for Darrieus Wind Turbines Using the Transition SST Model. *Processes 2021, 9(3),* 477. https://doi.org/10.3390/pr9030477
- Saad, A. S., AbdelSalam, A. M., Sakr, I. M., & El-Askary, W. A. (2017). Performance Analysis of a Helical Savonius Wind Turbine with Modified Rotor. *International Conference on Aerospace Sciences and Aviation Technology*, 17(Aerospace sciences and aviation technology, ASAT-17 – April 11-13, 2017), 1-14. https://doi.org/10.21608/ASAT.2017.22459
- Saini, G., & Saini, R. P. (2018). Numerical Investigation of the Effect of Blade Profile of a Darrieus Hydrokinetic Turbine. 2018 5th IEEE

- Uttar Pradesh Section International Conference on Electrical, Electronics and Computer Engineering, UPCON 2018. https://doi.org/10.1109/UPCON.2018.8597073
- Saini, G., & Saini, R. P. (2020). Comparative investigations for performance and self-starting characteristics of hybrid and single Darrieus hydrokinetic turbine. *Energy Reports*, 6, 96–100. https://doi.org/10.1016/j.egyr.2019.11.047
- Saryazdi, S. M. E., & Boroushaki, M. (2018). 2D numerical simulation and sensitive analysis of H-darrieus wind turbine. *International Journal of Renewable Energy Development*, 7(1), 23–34. https://doi.org/10.14710/ijred.7.1.23-24
- Tan, K. W., Kirke, B., & Anyi, M. (2021). Small-scale hydrokinetic turbines for remote community electrification. *Energy for Sustainable Development*, 63, 41–50. https://doi.org/10.1016/J.ESD.2021.05.005
- Tigabu, M. T., Khalid, M. S. U., Wood, D., & Admasu, B. T. (2022). Some effects of turbine inertia on the starting performance of vertical-axis hydrokinetic turbine. *Ocean Engineering*, 252, 111143. https://doi.org/10.1016/J.OCEANENG.2022.111143
- Vargas, J. A., Clavijo, F. V., & Torres Gómez, C. (2016). Desarrollo del prototipo de un hidrogenerador eléctrico como alternativa de generación de energía limpia en zonas rurales Development of the prototype of an electric hydro generator as an alternative for generating clean energy in rural areas. *Ingeniare*, 12(20), 91–101. https://doi.org/10.18041/1909-2458/ingeniare.20.411
- Wardhana, W., & Fridayana, E. N. (2020). Aerodynamic Performance Analysis of Vertical Axis Wind Turbine (VAWT) Darrieus Type H-Rotor using Computational Fluid Dynamics (CFD) Approach. December, 5–11. https://doi.org/10.5220/0008542700050011
- Welsby, D., Price, J., Pye, S., & Ekins, P. (2021). Unextractable fossil fuels in a 1.5 °C world. *Nature 2021 597:7875*, *597*(7875), 230–234. https://doi.org/10.1038/s41586-021-03821-8
- XM. (2022). 3.72% aumentó en febrero la demanda de energía eléctrica en Colombia - BNamericas. Bnamericas. https://www.bnamericas.com/es/noticias/372-aumento-en-febrero-la-demanda-de-energia-electrica-en-colombia.
- Yadav, P. K., Kumar, A., & Jaiswal, S. (2023). A critical review of technologies for harnessing the power from flowing water using a hydrokinetic turbine to fulfill the energy need. *Energy Reports*, 9, 2102–2117. https://doi.org/10.1016/J.EGYR.2023.01.033
- Yakhot, V., Orszag, S. A., Thangam, S., Gatski, T. B., & Speziale, C. G. (1992). Development of turbulence models for shear flows by a double expansion technique. *Physics of Fluids A: Fluid Dynamics*, 4(7), 1510–1520. https://doi.org/10.1063/1.858424
- Yunus Cengel, J. C. (2006). Mecánica de fluidos Fundamentos y aplicaciones.
 - https://books.google.com.co/books?id=higREQAAQBAJ



© 2025. The Author(s). This article is an open access article distributed under the terms and conditions of the Creative Commons Attribution-ShareAlike 4.0 (CC BY-SA) International License (http://creativecommons.org/licenses/by-sa/4.0/)